Research Article

Single-Fed Broadband CP Bidirectional Antenna with Double-Layer Diagonally Aligned Plates for Universal UHF-RFID Applications

Sitthichai Dentri,[1] Khanet Pookkapund,[2] Bancha Luadang,[3] Prayoot Akkaraekthalin,[4] and Chuwong Phongcharoenpanich [iD][2]

[1]*Research Center of Innovation Digital and Electromagnetic Technology (iDEMT), College of Industrial Technology, King Mongkut's University of Technology North Bangkok, Bangkok, Thailand*
[2]*Faculty of Engineering, King Mongkut's Institute of Technology Ladkrabang, Bangkok, Thailand*
[3]*Faculty of Engineering, Rajamangala University of Technology Rattanakosin, Nakhon Pathom, Thailand*
[4]*Department of Electrical and Computer Engineering, Faculty of Engineering, King Mongkut's University of Technology North Bangkok, Bangkok, Thailand*

Correspondence should be addressed to Chuwong Phongcharoenpanich; chuwong.ph@kmitl.ac.th

This research proposes a single-fed broadband circularly polarized (CP) bidirectional antenna operable in 840–960 MHz frequency band for readers of universal UHF-RFID applications. The proposed antenna is comprised of upper-layer conductor, lower-layer conductor, and wall patches. The upper-layer conductor consists of two diagonally aligned rectangular copper plates with a feeding gap at the center, and the lower-layer conductor is of two diagonally adjoined rectangular plates. The upper- and lower-layer conductors are adjoined with the wall patches. The diagonal alignment technique of the upper- and lower-layer plates was used to realize circular polarization and improve 3-dB axial ratio (AR) bandwidth. The double layers were deployed to improve impedance bandwidth ($|S_{11}| < -10$ dB) and achieve bidirectional radiation pattern. The simulated impedance bandwidth and 3-dB AR bandwidth were 772.19–1014.6 MHz (27.13%) and 675–1000 MHz (38.80%), and the corresponding measured results were 759–1011 MHz (28.47%) and 648–1110 MHz (52.55%). The simulated LHCP/RHCP half-power beamwidth (HPBW), 3-dB AR beamwidth, and gain were $56° – 90°/54° – 92°$, $60° – 104°$, and 4.94 – 5.89 dBic, while the corresponding measured results were $52° – 98°/62° – 97°$, $96° – 126°$, and 4.28 – 5.72 dBic. As a result, the single-fed broadband CP bidirectional antenna is applicable to universal UHF-RFID readers. Besides, the novelty of this research lies in the use of diagonal alignment of conducting plates to achieve circular polarization and wider AR bandwidth.

1. Introduction

Radio frequency identification (RFID) technology is commonly utilized for wireless multiaccess identification and tracking in logistics, livestock farming, and toll collection [1, 2]. Ultrahigh frequency (UHF) RFID varies from country to country. The RFID frequency band in China is 840.5 – 844.5 MHz, 920 – 925 MHz in Thailand, and 902 – 928 MHz in the US. Meanwhile, the Federal Communications Commission's (FCC) universal RFID frequency band is 860 – 960 MHz. RFID reader antennas have to be able to communicate between readers and tags, independent of tag orientation. To satisfy this requirement, CP antennas are thus necessary [3, 4]. Meanwhile, bidirectional radiation is ideal for identification and tracking moving objects in a tunnel or on a conveyor belt [5].

Previous research proposed techniques to realize wideband CP antennas [6–14]. In [6], a CP slot antenna was proposed, and the antenna could achieve a fractional CP bandwidth (FCPBW) over 40% and 3-dB AR bandwidth of

48%. However, the antenna gain was comparably low (4.2 dBic). In [7], a novel broadband CP antenna with square slot was proposed for UHF-RFID applications. The CP antenna achieved impedance bandwidth of 142 MHz (15.3% at 931 MHz) and 3-dB AR bandwidth of 166 MHz (17.7% at 940 MHz). In [8], a compact CP slot antenna was proposed to improve impedance matching and broadband CP. In [9], a simple rotational symmetric printed bow-tie dipole structure was proposed for frequency-selective polarization antenna (FSPA), and the antenna could achieve impedance bandwidth of 1.9 – 5.65 GHz (98.7%) and 3-dB AR bandwidths of 8.3% (2.3 – 2.5 GHz) and 13.3% (4.9 – 5.6 GHz). In [10], a novel antenna was proposed to achieve bidirectionally tilted circular polarization. In [11], a CP monopole antenna based on natural boundary conditions was proposed and could achieve 3-dB AR bandwidths of 5.38% and 2.84%. In [12], a geometrically simple structure for broadband CP applications could achieve very wide impedance bandwidth of 89% with 82% CP bandwidth but low antenna gain (<5 dBic). In [13], a compact broadband dual-band CP square slot antenna was proposed for worldwide UHF-RFID handheld readers and L2 and L5 global positioning system (GPS). The proposed antenna achieved impedance bandwidth of 716 – 1268 MHz (552 MHz) and 3-dB AR bandwidth of 824 – 1388 MHz (564 MHz). However, the antenna gain was relatively low (<5 dBic). In [14], three low-profile ultra-wideband (UWB) circularly polarized slot antennas were proposed for UWB indoor wireless access. However, the antennas suffered from bulkiness.

This research proposes a single-fed broadband CP bidirectional antenna that efficiently covers the universal UHF-RFID frequency band. The proposed folded antenna is comprised of upper-layer conductor, lower-layer conductor, and wall patches. The upper-layer conductor consists of two diagonally aligned rectangular copper plates with a feeding gap at the center, and the lower-layer conductor is of two diagonally adjoined rectangular plates. The upper- and lower-layer conductors are adjoined with the wall patches.

The organization of the research is as follows: Section 1 is the introduction. Section 2 details the design of the antenna structure. Section 3 deals with the simulation and measurement results, and Section 4 discusses the parametric study analysis. The concluding remarks are provided in Section 5.

2. Antenna Structure

Figure 1 illustrates the geometry and parameters of the single-fed broadband CP bidirectional antenna for universal UHF-RFID applications. The proposed folded antenna comprises upper-layer conductor, lower-layer conductor, and wall patches. The upper-layer conductor consists of two diagonally aligned rectangular plates with a feeding gap at the center, and the lower-layer conductor is of two diagonally adjoined rectangular plates. The upper- and lower-layer conductors are adjoined with the wall patches. Air is used as the substrate to achieve high gain, broad bandwidth, and low cost.

The proposed broadband CP bidirectional antenna was fabricated from copper sheet of 1 mm in thickness. The selected copper thickness (1 mm) helped strengthen the antenna structure. The dimension of the proposed antenna was $146 \, mm \times 275 \, mm \times 10 \, mm$ $(W \times L \times h)$. The antenna was excited by a $50 \, \Omega$ coaxial feed. The width (W_{tf}) and length (L_{ty}) of the upper-layer rectangular patch were 74 and 138 mm, and the width (W_{bf}) and length (L_{by}) of the lower-layer rectangular patch were 74 and 137.5 mm. The upper- and lower-layer rectangular patches were staggered by 1 mm. The feeding gap (δ) was 3 mm fed by a coaxial cable. An N-type connector was connected to the coaxial cable hidden beneath the upper-layer plate. Table 1 tabulates the antenna parameters and optimal dimensions of the proposed broadband CP bidirectional antenna simulated by CST Microwave Studio [15].

3. Parametric Study Analysis

3.1. Evolutionary Stages of the Antenna. Figure 2 shows three evolutionary stages of the proposed antenna: two diagonally aligned rectangular plates (upper-layer plates), the diagonally aligned rectangular plates with wall patches, and broadband CP bidirectional antenna. The initial length of the proposed antenna (L) was approximately $\lambda/4$ in order to achieve AR < 3 dB, where λ is the wavelength of the center frequency (900 MHz). The optimal length of the antenna was 275 mm. The wall patch dimension and feeding gap were optimized (Table 1). Circular polarization was thus realized as current flowed from the upper-layer plates to the wall patches and to the lower-layer plates. The time (t) for the current to flow from one end to the other end of the wall patch was different, with 90° phase difference.

Figures 3(a)–3(c) show the simulated $|S_{11}|$, impedance, and AR pattern of the proposed antenna in the three evolutionary stages. The double-layered structure of the proposed antenna resulted in AR bandwidth lower than 3 dB for the universal UHF-RFID frequency band. In Figure 3, Stage 1 of the antenna evolution achieved AR bandwidth close to 3 dB, and resistance and reactance were reduced by using the wall patches in Stage 2. In Stage 3, the resistance, reactance, and AR bandwidth were further reduced by incorporating the lower-layer rectangular plates.

3.2. Width of the Proposed Antenna (W). Figures 4(a) and 4(b) show the simulated $|S_{11}|$ and AR of the proposed antenna under different antenna widths (W): 140, 143, 146, 149, and 152 mm. The simulation results revealed that the variation in W had minimal impact on $|S_{11}|$ but significant effect on AR bandwidth, especially in higher-frequency range. The AR bandwidth became narrower as W increased.

Specifically, as W decreased, the impedance bandwidth $(|S_{11}| < -10 \, dB)$ became wider, and AR amplitude deteriorated. On the other hand, as W increased, the impedance bandwidth shifted to lower frequency and became narrower, and AR amplitude deteriorated. The AR bandwidth nonetheless covered the universal UHF-RFID frequency band, independent of W.
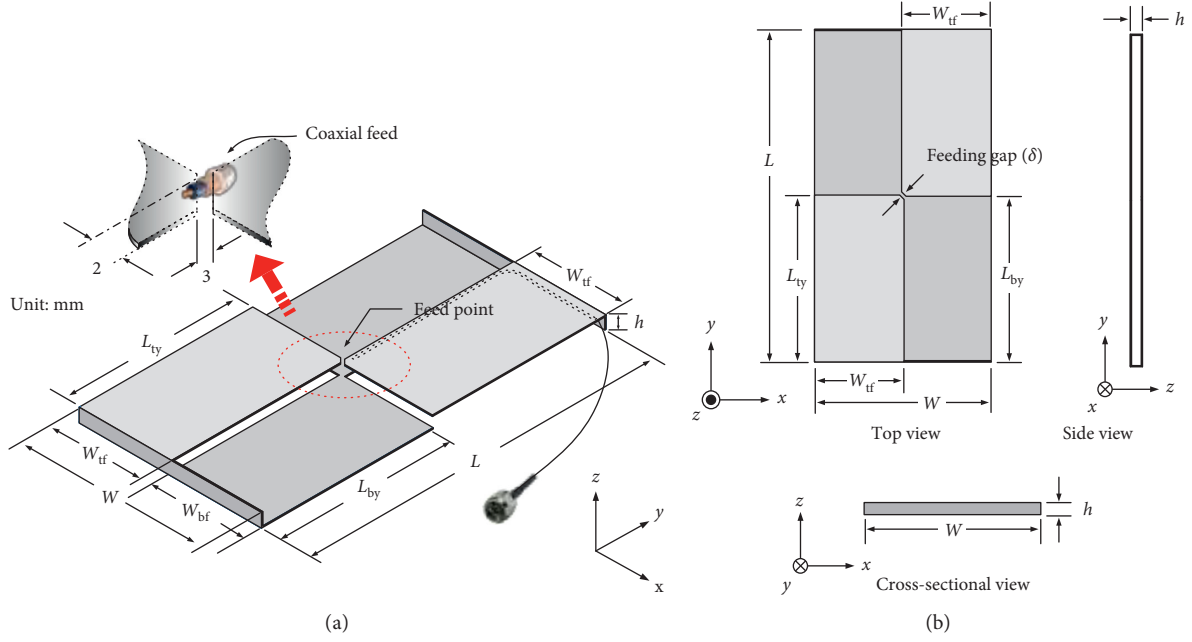
FIGURE 1: The geometry of the proposed broadband CP bidirectional antenna. (a) Perspective view, (b) multiview rendition.

TABLE 1: Parameters of single-fed broadband circularly polarized bidirectional antenna operable at universal UHF-RFID frequency band.

Symbol	Parameters	Optimal dimension (mm)
W	Width of antenna	146
L	Length of antenna	275
H	Height of wall patch	10
W_{tf}	Width of upper rectangular patch	74
W_{bf}	Width of lower rectangular patch	74
L_{ty}	Length of upper rectangular patch	138
L_{by}	Length of lower rectangular patch	137.5
Δ	Feeding gap	3
—	Copper thickness	1

The optimal width (W) of the proposed antenna was 146 mm, given that the AR bandwidth effectively covered the entire UHF-RFID frequency band. Besides, variations in W had no effect on the antenna gain in the lower frequency range and minimal effect in the upper frequency range. As a result, no graphical presentation of the effect of W on the antenna gain was provided.

3.3. Length of Proposed Antenna (L).

Figures 5(a) and 5(b) show the simulated $|S_{11}|$ and AR of the proposed antenna under variable antenna lengths (L): 265, 270, 275, 280, and 285 mm. Given the optimal antenna length (L) of 275 mm, as L increased (280 and 285 mm), the AR bandwidth of the antenna deteriorated and became wider. As L decreased (265 and 270 mm), the AR bandwidth became narrower. Meanwhile, as L decreased, the impedance bandwidth ($|S_{11}|$ < −10 dB) shifted to the higher-frequency range with slightly improved antenna gain. As L increased, the impedance

bandwidth deteriorated with slightly lower antenna gain. Since variations in L had negligible effect on the antenna gain, no graphical presentation of the effect of L on the antenna gain was provided.

3.4. Height of Wall Patch (h).

Figures 6(a) and 6(b) illustrate the simulated $|S_{11}|$ and AR of the proposed antenna under variable wall heights (h): 6, 8, 10, 12, and 14 mm. Given the optimal wall height of 10 mm (Table 1), as h increased (12 and 14 mm), the AR bandwidth of the antenna improved and became narrower. As h decreased (6 and 8 mm), the AR bandwidth became wider. In addition, as h increased (12 mm), the impedance bandwidth ($|S_{11}|$ < −10 dB) slightly shifted at the same frequency range with steady antenna gain. As h varied (6, 8, and 14 mm), the impedance bandwidth deteriorated with slightly lower antenna gain. Since variations in h had negligible effect on the antenna gain, no graphical presentation of the effect of h on the antenna gain was provided.

3.5. Length of Feeding Gap (δ).

Given the optimal feeding gap (δ) at the center of the upper-layer conductor of 3 mm (Table 1), the simulated impedance bandwidth ($|S_{11}|$ < −10 dB) covered the universal UHF-RFID frequency band, as shown in Figure 7(a). Figures 7(a) and 7(b) illustrate the simulated $|S_{11}|$ and AR of the proposed antenna under variable feeding gaps (δ): 1, 3, 5, 7, and 9 mm. In Figure 7(a), as δ increased (5, 7, and 9 mm), the impedance bandwidth shifted to the lower frequency range, and the impedance bandwidth shifted to the higher-frequency range as δ decreased (1 mm). Nonetheless, the AR bandwidth was below 3 dB, independent of δ, as shown in Figure 7(b).
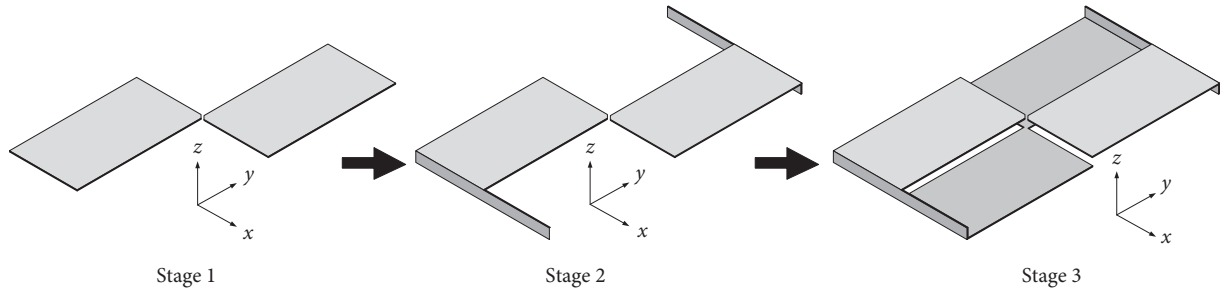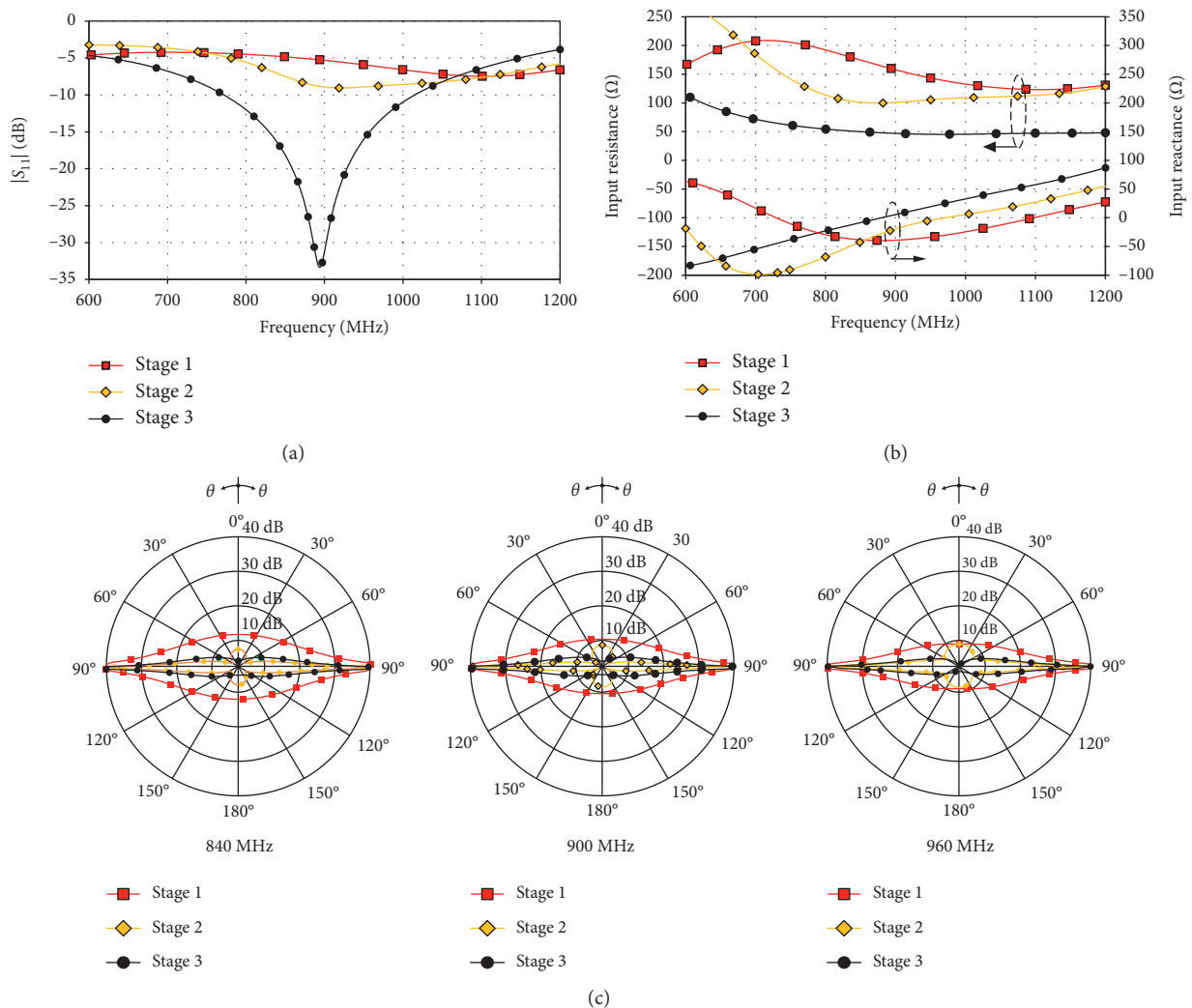
FIGURE 2: Evolutionary stages of the broadband CP bidirectional antenna.

FIGURE 3: The simulated results of the proposed antenna under three evolutionary stages: (a) $|S_{11}|$, (b) impedance, (c) AR patterns.

3.6. The Width of Upper Rectangular Plate (W_{tf}). The width of upper rectangular patch (W_{tf}) was optimized to improve the AR bandwidth to cover the universal UHF-RFID frequency band. Figures 8(a) and 8(b) illustrate the simulated $|S_{11}|$ and AR of the proposed antenna under variable widths of upper rectangular patch (W_{tf}): 34, 54, 74, 94, and 114 mm. Given the optimal width of upper rectangular patch (W_{tf}) of 74 mm (Table 1), the simulated impedance bandwidth ($|S_{11}| < -10$ dB) covered the universal UHF-RFID frequency band, as shown in Figure 8(a). The simulated impedance bandwidth and AR bandwidth outside of the optimal W_{tf} (34, 54, 94, and 114 mm) dramatically deteriorated, as shown in Figures 8(a) and 8(b).
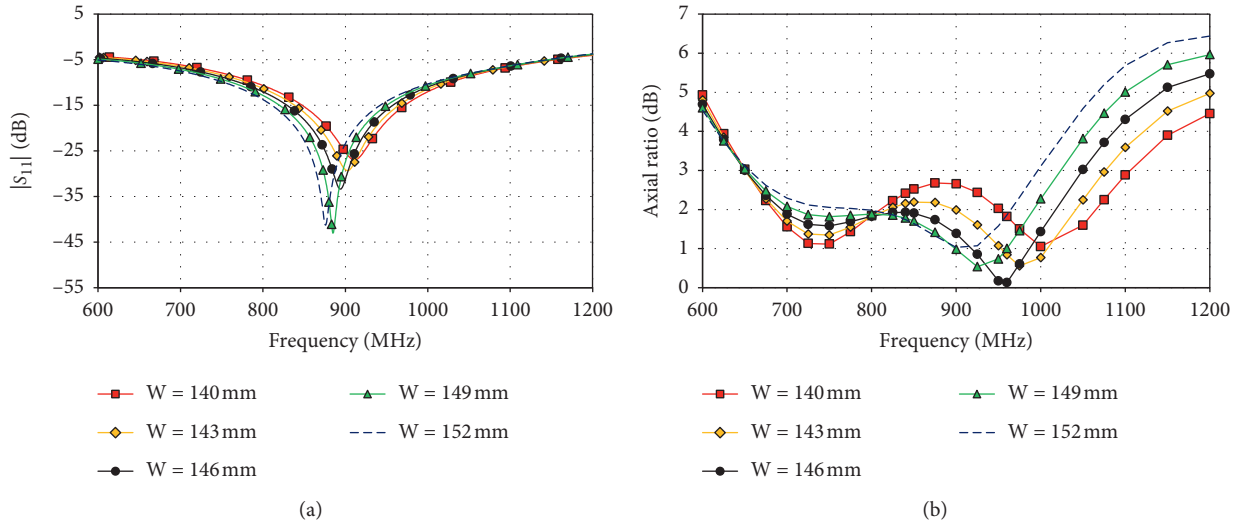
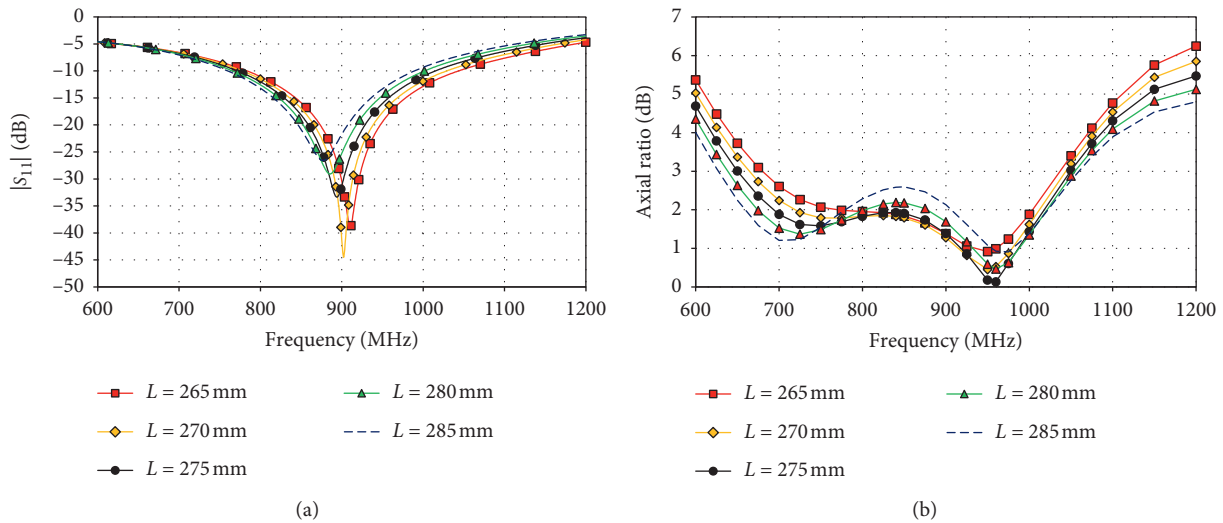FIGURE 4: Simulation results under variable antenna widths (W): (a) $|S_{11}|$, (b) axial ratio.

FIGURE 5: Simulation results under variable antenna lengths (L): (a) $|S_{11}|$, (b) axial ratio.

3.7. The Width of Lower Rectangular Plate (W_{bf}). Figures 9(a) and 9(b) illustrate the simulated $|S_{11}|$ and AR of the proposed antenna under variable widths of lower rectangular plate (W_{bf}): 34, 54, 74, 94, and 114 mm. Given the optimal width of lower rectangular patch (W_{bf}) of 74 mm (Table 1), the simulated impedance bandwidth ($|S_{11}| < -10$ dB) covered the universal UHF-RFID frequency band, as shown in Figure 9(a). The simulated impedance bandwidth outside of the optimal W_{bf} (34, 54, 94, and 114 mm) shifted to the lower frequency range, while the AR bandwidth deteriorated and became greater than 3 dB, thereby failing to achieve circular polarization, as shown in Figures 9(a) and 9(b).

3.8. The Length of Upper Rectangular Patch (L_{ty}). The length of upper rectangular patch (L_{ty}) was optimized to improve the AR bandwidth to cover the universal UHF-RFID frequency band. Figures 10(a) and 10(b) illustrate the simulated $|S_{11}|$ and AR of the proposed antenna under variable lengths of upper rectangular patch (L_{ty}): 58, 95, 138, 178, and 218 mm. Given the optimal length of upper rectangular patch (L_{ty}) of 138 mm (Table 1), the simulated impedance bandwidth ($|S_{11}| < -10$ dB) covered the universal UHF-RFID frequency band, as shown in Figure 10(a). Under L_{ty} of 58, 95, 178, and 218 mm, the simulated impedance bandwidth failed to cover the
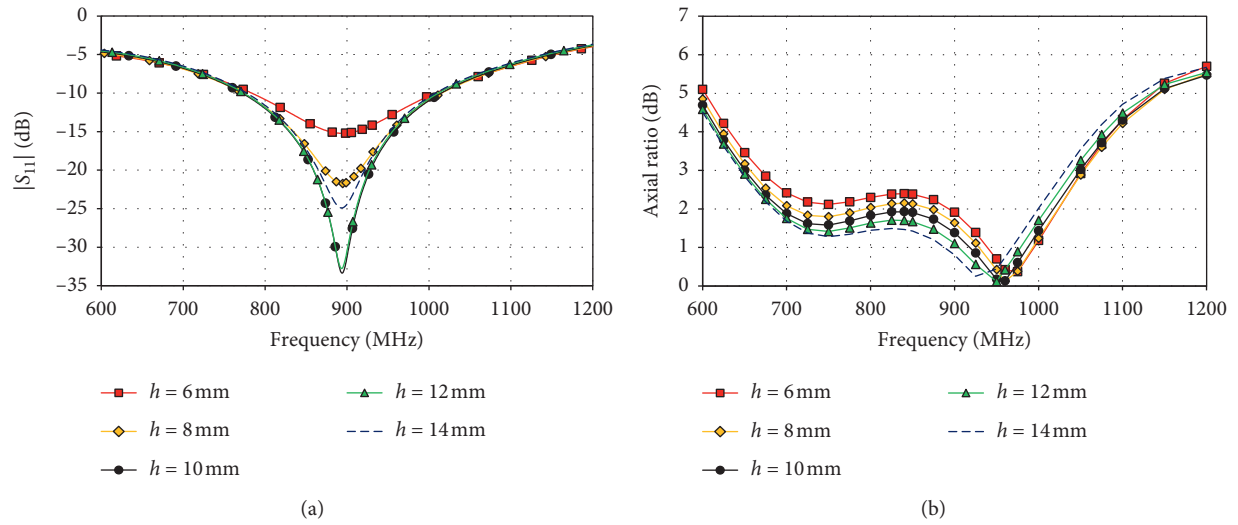
(a)

(b)

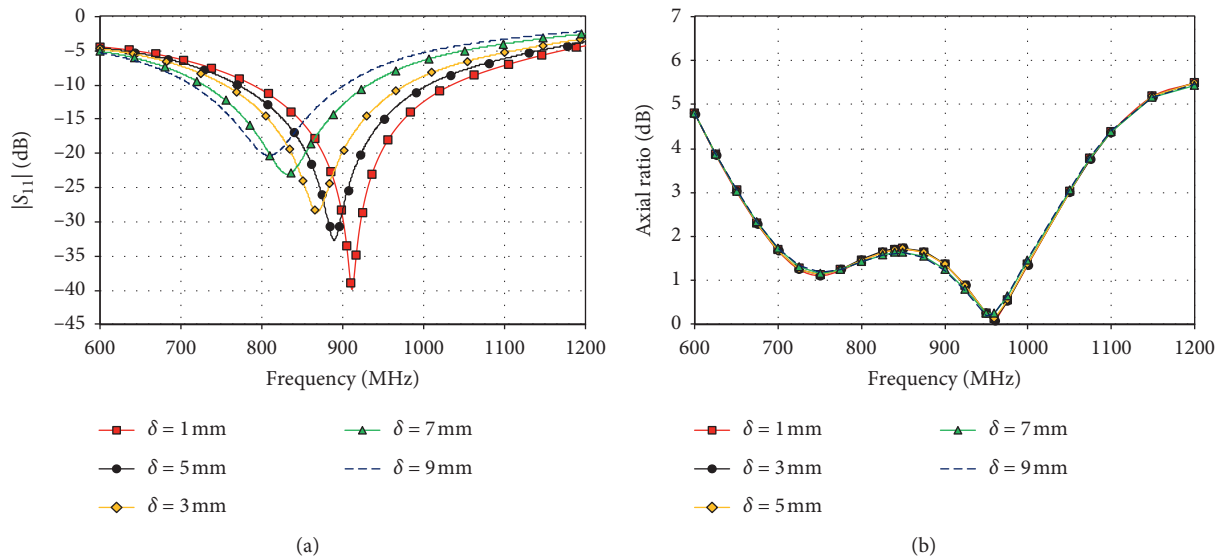Figure 6: Simulation results under variable wall heights (h): (a) $|S_{11}|$, (b) axial ratio.

(a)

(b)

Figure 7: Simulation results under variable feeding gap (δ): (a) $|S_{11}|$, (b) axial ratio.
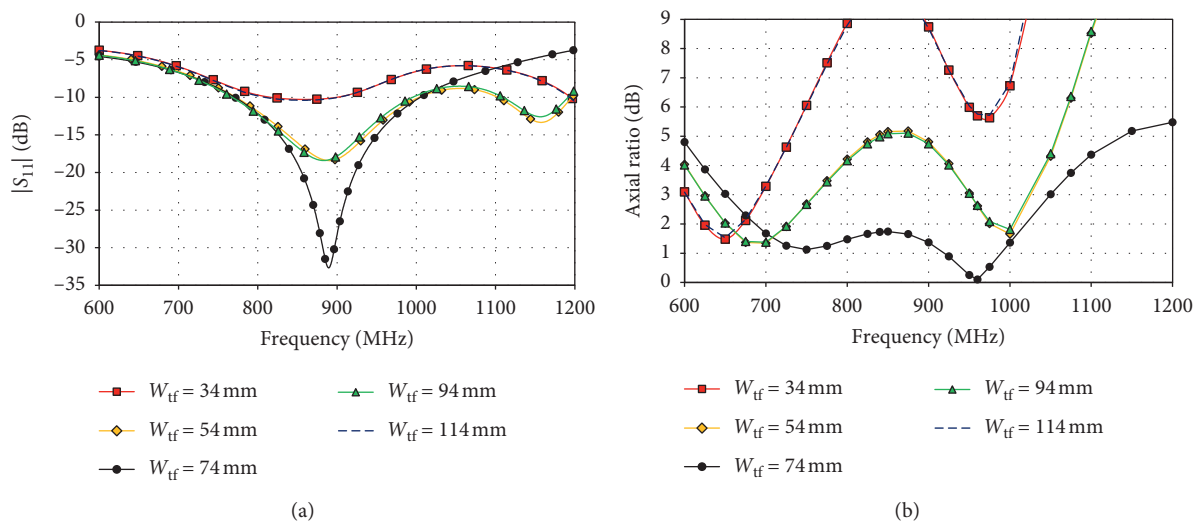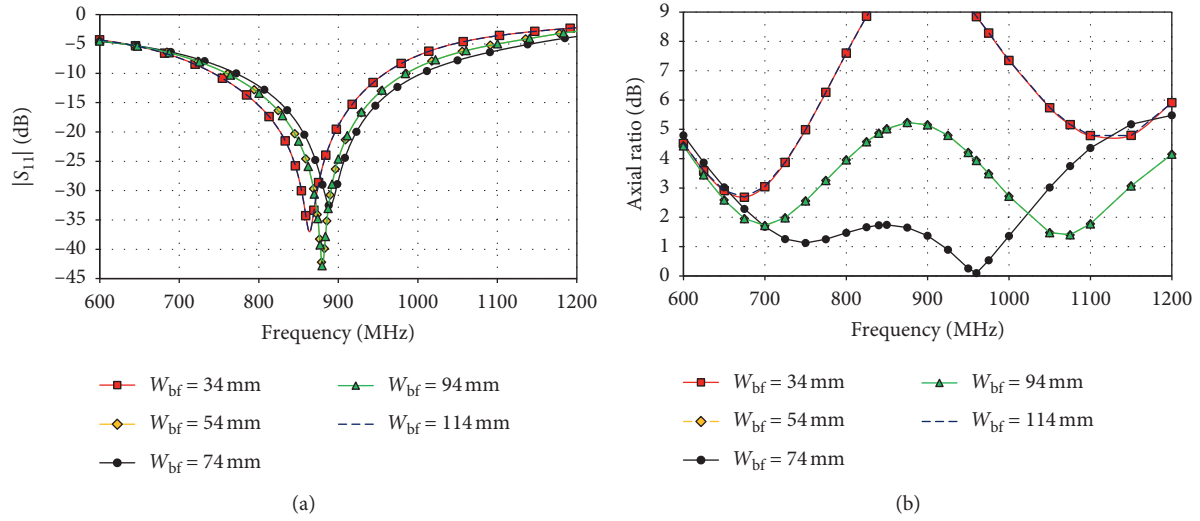

(a)

(b)

Figure 8: Simulation results under variable widths of upper rectangular plate ($(W)_{tf}$): (a) $|S_{11}|$, (b) axial ratio.

FIGURE 9: Simulation results under variable widths of lower rectangular plate ($(W)_\mathrm{bf}$): (a) $|S_{11}|$, (b) axial ratio.
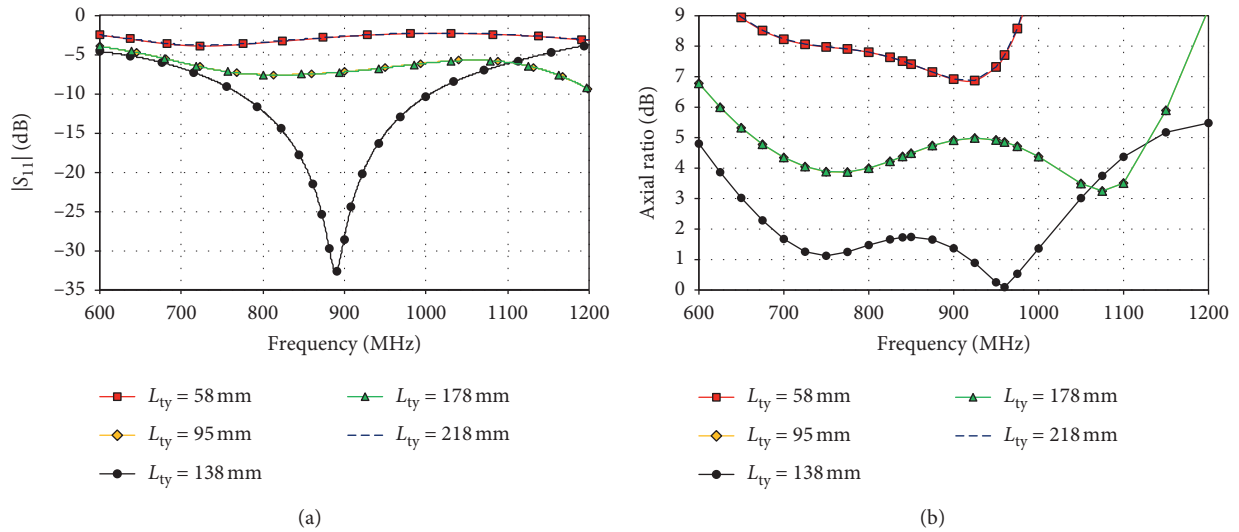

FIGURE 10: Simulation results under variable lengths of upper rectangular patch ($(L)_\mathrm{ty}$): (a) $|S_{11}|$, (b) axial ratio.

universal UHF-RFID frequency band, and the AR bandwidth deteriorated and became greater than 3 dB, thus failing to achieve circular polarization, as shown in Figures 10(a) and 10(b).

3.9. The Length of Lower Rectangular Patch (L_{by}).
Figures 11(a) and 11(b) show the simulated $|S_{11}|$ and AR of the proposed antenna under variable lengths of lower rectangular plate (L_{by}): 57.5, 94.5, 137.5, 177.5, and 217.5 mm. Given the optimal length of lower rectangular patch (L_{by}) of 137.5 mm (Table 1), the simulated impedance bandwidth ($|S_{11}| < -10$ dB) covered the universal UHF-RFID frequency band, as shown in Figure 11(a). The simulated impedance bandwidth outside of the optimal L_{by} (57.5, 94.5, 177.5, and 217.5 mm) shifted to the lower frequency range and deteriorated, while the AR bandwidth deteriorated and

became greater than 3 dB, thus failing to achieve circular polarization, as shown in Figures 11(a) and 11(b).

3.10. Vector Current Distribution on the Upper-Layer Diagonally Aligned Rectangular Plates.
Figure 12 illustrates the simulated vector current distribution on the upper-layer diagonally aligned rectangular plates at the center frequency of 900 MHz relative to time (t). The current from the feeding point at the center of the upper-layer plates was distributed on the upper-layer conductor surface with the same magnitude and 90° phase difference, independent of time (t). The direction of surface current on the upper-layer diagonally aligned rectangular plates was counterclockwise relative to time (t). Meanwhile, the surface current on the lower-layer diagonally adjoined rectangular plates was clockwise relative to time (t). The directions of surface current on the upper- and lower-
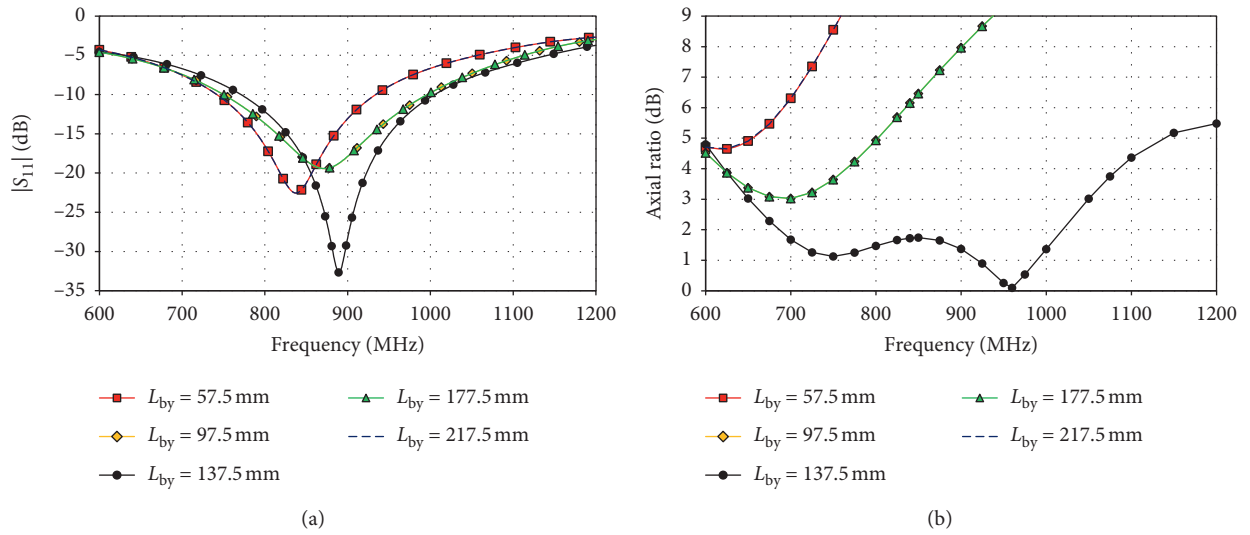
(a)

(b)

FIGURE 11: Simulation results under variable lengths of lower rectangular patch (L_{by}): (a) $|S_{11}|$, (b) axial ratio.
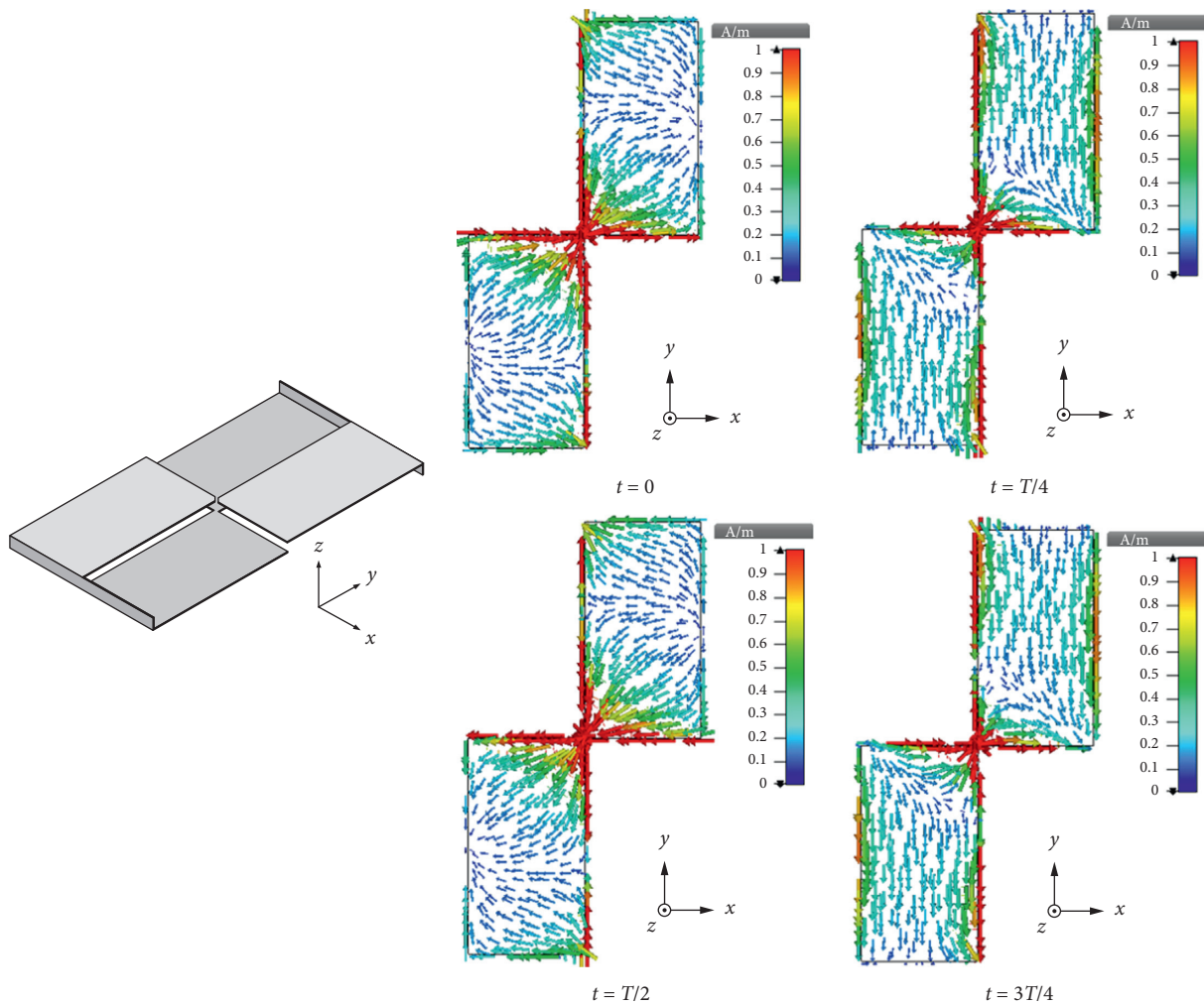

FIGURE 12: Simulated vector current distribution on the upper-layer diagonally aligned rectangular plates at the center frequency of 900 MHz.
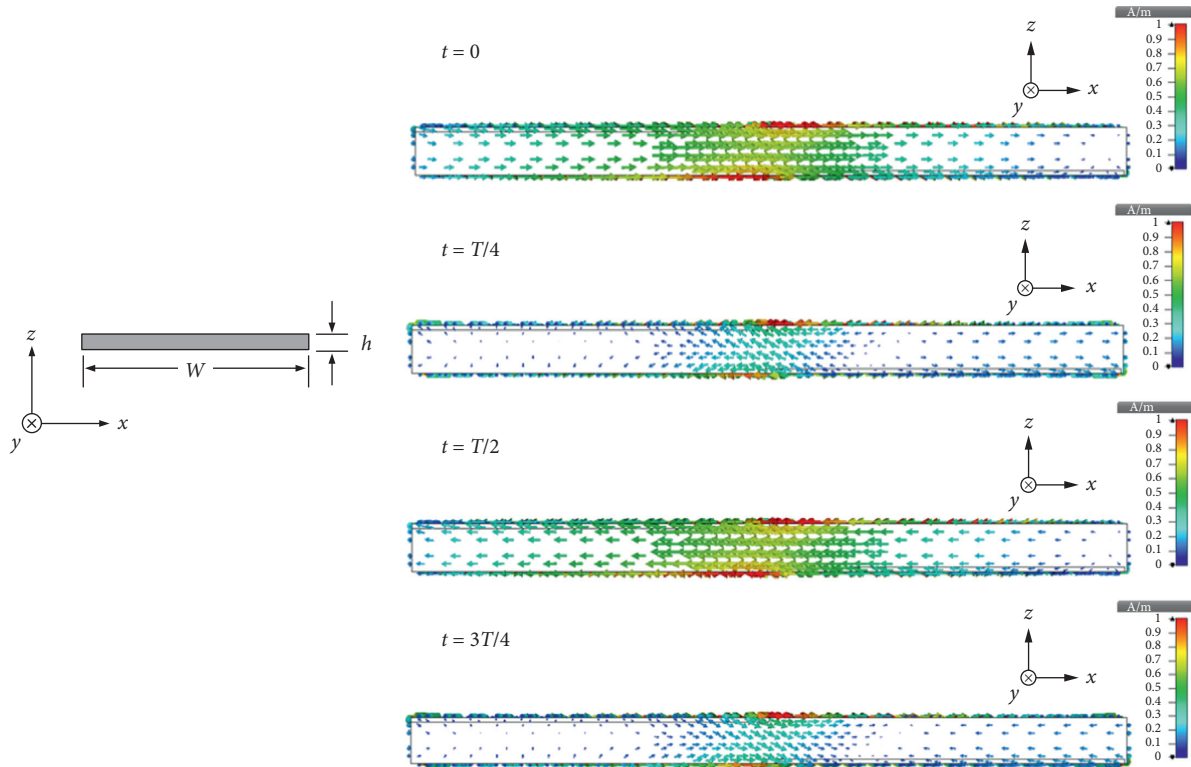
FIGURE 13: Simulated vector current distribution on one end of the wall patch at the center frequency of 900 MHz.

layer rectangular plates at 840 and 960 MHz resembled those at the center frequency. The concurrent use of upper- and lower-layer diagonally aligned rectangular plates thus resulted in circular polarization.

Figure 13 shows the simulated current distribution on one end of the wall patch at the center frequency of 900 MHz relative to time (t). The direction of surface current was counterclockwise, while that of the other end of the wall patch was clockwise. The opposite directions of surface current resulted in circular polarization. The directions of surface current on the both ends of the wall patch at 840 and 960 MHz resembled those at the center frequency.

4. Simulation and Measurement Results

A prototype antenna was fabricated based on the optimal dimensions (Table 1), and far-field experiments were carried out in an anechoic chamber using HP8720C network analyzer. Figure 14 depicts the prototype broadband CP bidirectional antenna.

Figure 15(a) illustrates the simulated and measured $|S_{11}|$ of the broadband CP bidirectional antenna. The simulated and measured $|S_{11}|$ (≤ -10 dB) covered the frequency range of 772.19 – 1014.6 MHz (27.13% bandwidth) and 759 – 1011 MHz (28.47% bandwidth), respectively, both of which encompassed the universal UHF-RFID frequency band of 840 – 960 MHz. The simulated and measured results were in good agreement. In Figure 15(b), the simulated and measured 3-dB AR bandwidth of the proposed antenna were 675 – 1000 MHz (38.80% AR
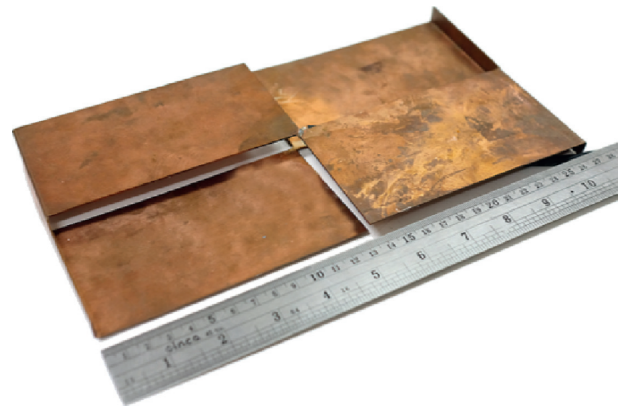

FIGURE 14: Photograph of the prototype broadband CP bidirectional antenna.

bandwidth) and 648 – 1110 MHz (52.55% AR bandwidth), respectively.

Figures 16(a)–16(c) show the simulated and measured x–z and y–z plane radiation patterns at 840, 900 (center frequency), and 960 MHz, respectively. The total radiation patterns were bidirectional in both planes with circular polarization. The radiation patterns were near-symmetrical in front-back boresight for the universal UHF-RFID frequency band. The CP pattern is LHCP in direction of 180° along the operating frequency band. The simulated LHCP half-power beamwidth (HPBW) in x–z and y–z planes at 840, 900, and
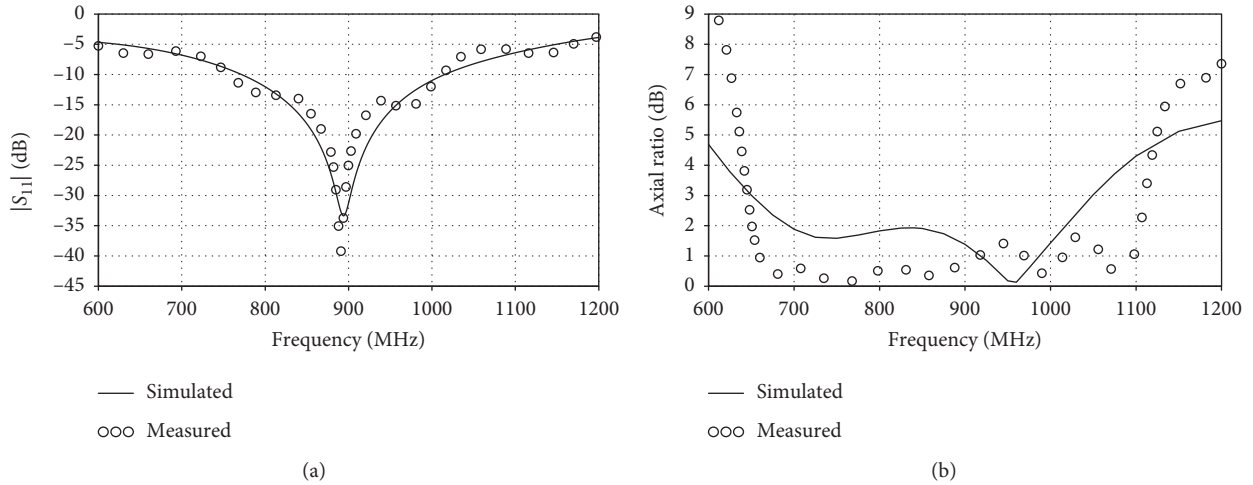
FIGURE 15: Simulated and measured results of the proposed antenna: (a) $|S_{11}|$, (b) axial ratio.
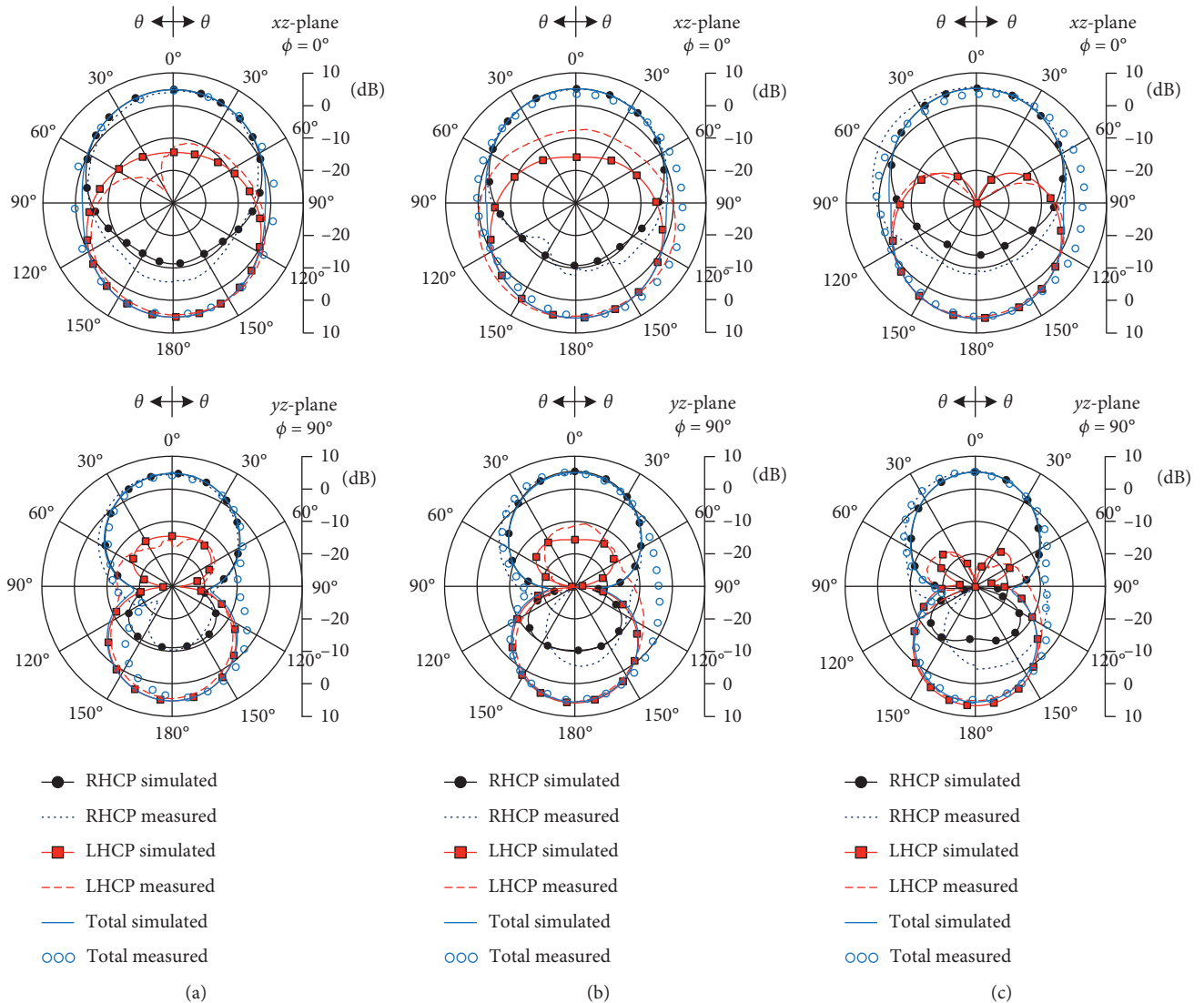

FIGURE 16: Simulated and measured x–z and y–z plane radiation patterns of the proposed antenna: (a) 840 MHz, (b) 900 MHz, (c) 960 MHz.
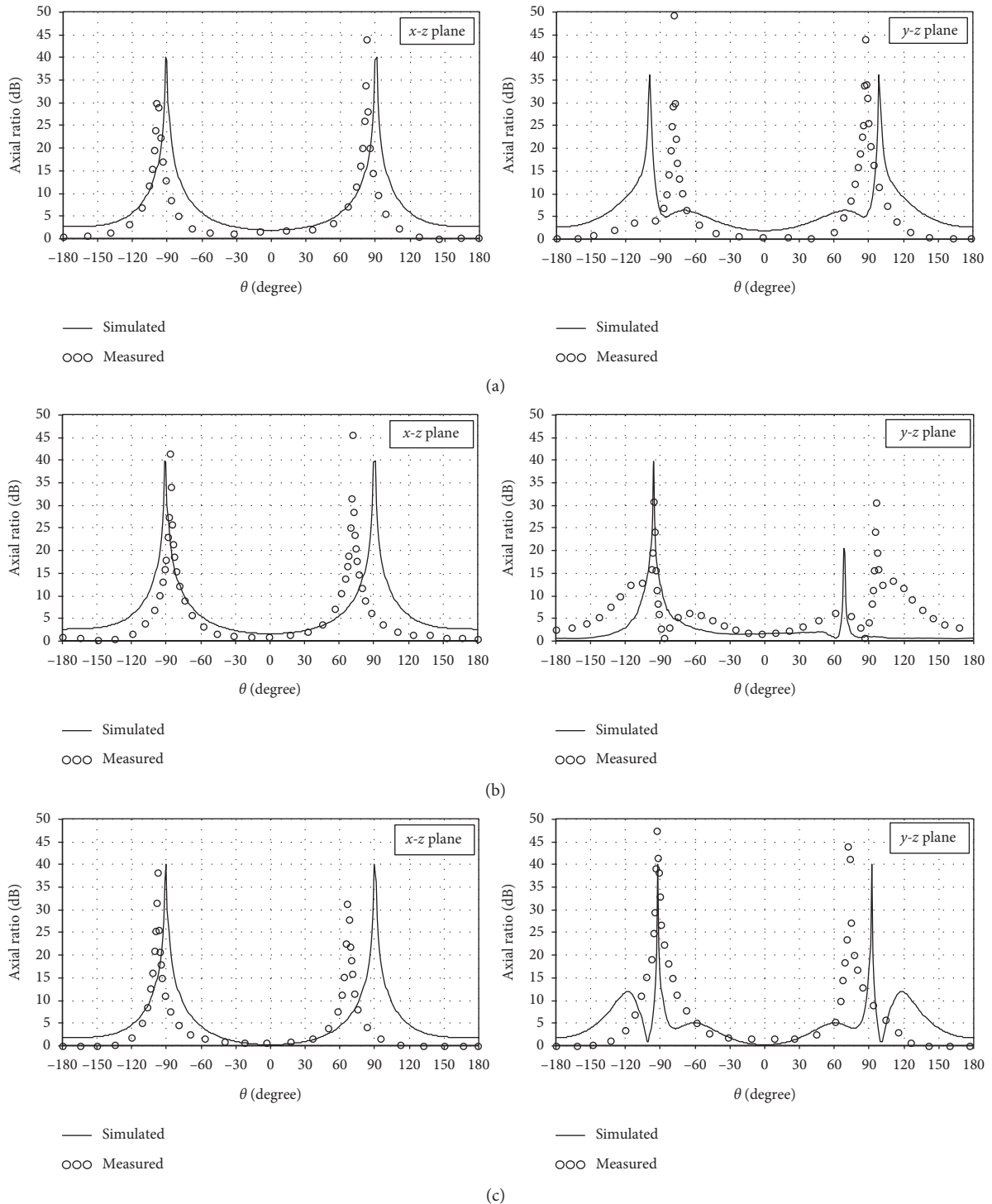
Figure 17: Simulated and measured *xz* and *yz* plane axial ratio relative to angle. (a) 840 MHz, (b) 900 MHz, (c) 960 MHz.

960 MHz was 90° and 56°; 86° and 56°; and 82° and 56°. The corresponding measured LHCP HPBW were 98° and 52°; 97° and 52°; and 88° and 56°. The RHCP pattern occurred in direction of 0°. The RHCP HPBW in *x–z* and *y–z* planes at 840, 900, and 960 MHz were 92° and 56°; 84° and 54°; and 76° and 54°. The corresponding measured RHCP HPBW were 79° and 62°; 97° and 63°; and 88° and 65°.

The simulated *xz* and *yz* plane 3-dB AR beamwidth at 840, 900, and 960 MHz was 76° and 60°; 80° and 62°; and 104° and 80°. The corresponding measured 3-dB AR beamwidth was 123° and 118°; 96° and 126°; and 117° and 97°, as shown in Figures 17(a)–17(c), respectively.

Figure 18 compares the simulated and measured realized gains of the proposed broadband CP bidirectional antenna. The
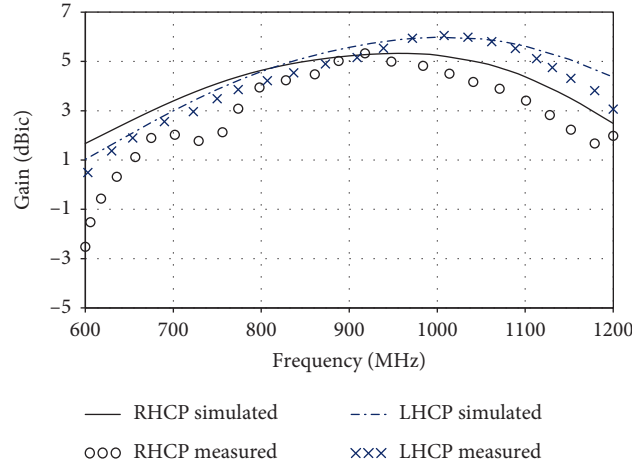
FIGURE 18: Simulated and measured antenna gain of the proposed broadband CP bidirectional antenna.

TABLE 2: Characteristics of the proposed antenna.

Characteristic		840 MHz		900 MHz		960 MHz	
		Simulated	Measured	Simulated	Measured	Simulated	Measured
$|S_{11}|$ (dB)		−16.56	−13.99	−30.87	−25.03	−14.6	−15.35
AR (dB)		1.92	0.46	1.38	0.79	0.13	1.36
LHCP gain (dBic)		5.05	4.66	5.57	5.16	5.89	5.72
RHCP gain (dBic)		4.94	4.28	5.22	5.2	5.32	4.89
LHCP HPBW (degree)	xz plane	90	98	86	97	82	88
	yz plane	56	52	56	52	56	56
RHCP HPBW (degree)	xz plane	92	79	84	97	76	88
	yz plane	56	62	54	63	54	65
		Simulated			Measured		
$|S_{11}| \leq -10$ dB bandwidth		772.19 – 1014.6 MHz, 27.13%			759 – 1011 MHz, 28.47%		
AR ≤ 3 dB bandwidth		675 – 1000 MHz, 38.8%			648 – 1110 MHz, 52.55%		
Global bandwidth (%)		675 – 1000 MHz, 38.8%			648 – 1011 MHz, 43.76%		
Pattern				Bidirectional			

TABLE 3: Comparison between previous studies and this current research.

References	Fractional bandwidth of $|S_{11}|$ (%)	Fractional bandwidth of AR (%)	Maximum gain (dBic)	Overall antenna dimension
[6]	51.36	48.80	4.20	0.405 λL × 0.405 λL × 0.005 λL at 2023 MHz
[7]	15.25	15.59	6.80	0.347 λL × 0.361 λL × 0.002 λL at 860 MHz
[8]	47.03	23.14	3.41	0.247 λL × 0.247 λL × 0.002 λL at 618 MHz
[9]	99.34	8.3, 13.3	2.1, 4.4	0.317 λL × 0.190 λL × 0.006 λL at 1900 MHz
[10]	46.68	6.19	8.00	0.520 λL × 0.988 λL × 0.260 λL at 1560 MHz
[11]	9.48	2.84	11.10	1.309 λL × 1.625 λL × 1.155 λL at 2310 MHz
[12]	89.66	82.00	3.30	0.373 λL × 0.240 λL × 0.023 λL at 3200 MHz
[13]	55.65	42.44	4.29	0.267 λL × 0.267 λL × 0.004 λL at 716 MHz
[14]	98.72	84.10	9.60	0.843 λL × 0.843 λL × 0.101 λL at 3370 MHz
Proposed antenna	28.47	52.55	5.89	0.369 λL × 0.696 λL × 0.025 λL at 759 MHz

simulated and measured RHCP realized gains were 4.94 – 5.32 dBic and 4.28 – 5.32 dBic, respectively. The corresponding LHCP gains were 5.05 – 5.89 dBic and 4.66 – 5.74 dBic, respectively, over the universal UHF-RFID frequency band. The simulated and measured RHCP maximum gains were 5.32 dBic at 960 MHz and 5.32 dBic at 915 MHz. The

corresponding LHCP maximum gains were 5.89 dBic at 960 MHz and 5.74 dBic at 951 MHz.

Table 2 compares the characteristics of the proposed antenna from simulated and measured results ($|S_{11}|$, AR, gain, HPBW, bandwidth, and pattern) along operating frequency band. The simulated and measured results are in good agreement.

5. Comparison between CP Bidirectional Antennas

The overall dimension of the proposed single-fed broadband CP bidirectional antenna is 146 mm × 275 mm × 10 mm excluding the coaxial cable and N-type connector. The coaxial cable and the connector were required to feed radio frequency (RF) signal to the upper-layer diagonally aligned rectangular plates, and the length of the coaxial cable was $\lambda/4$ at the center frequency.

Table 3 compares the proposed broadband CP bidirectional antenna with existing CP bidirectional antennas. In [6, 12], the higher-frequency antennas achieved improved impedance and AR bandwidths but lower antenna gain. In [7], the antenna achieved higher gain but narrower impedance and AR bandwidths. In [8, 13], the antennas were smaller than the proposed antenna but achieved lower antenna gain. In [9], the antenna had narrower AR bandwidth and lower antenna gain. In [11, 14], the antennas achieved higher gain but suffered from bulkiness. For antennas operable in the universal UHF-RFID frequency band (840–960 MHz), the proposed single-fed broadband CP bidirectional antenna efficiently achieves high bidirectional antenna gain with compact size.

6. Conclusions

This experiment research introduced a technique of diagonal alignment of two rectangular copper plates to generate circular polarization and improve 3-dB AR bandwidth, where the principle of circular polarization is proved by surface current analysis. Moreover, double layers of diagonally aligned rectangular plates were adopted to improve impedance bandwidth ($S_{11}| < -10$ dB) and achieve bidirectional radiation pattern. According to the characteristics that were analyzed and described in detail of the parametric study section, the prototype antenna was fabricated based on the optimal dimensions, and far-field experiments were carried out in an anechoic chamber using HP8720C network analyzer. The impedance bandwidth, 3-dB AR bandwidth, LHCP/RHCP HPBW, 3-dB AR beamwidth, and gain of the prototype UHF-RFID antenna were 759–1011 MHz (28.74%), 648–1110 MHz (52.55%), $52°–98°/62°–97°$, $96°–126°$, and 4.28–5.72 dBic, respectively. The proposed single-fed broadband CP bidirectional antenna is thus universally applicable to UHF-RFID readers of varying geographical areas.

Data Availability

The data used to support the findings of this study are available from the corresponding author upon request.

Conflicts of Interest

The authors declare that there are no conflicts of interest regarding the publication of this paper.

References

[1] K. Finkenzeller, "*RFID Handbook: Fundamentals and Applications in Contactless Smart Cards and Identification,*" John Wiley and Sons, Ltd., Hoboken, NJ, USA, 2003.

[2] Y. Yao, C. Cui, J. Yu, and X. Chen, "A meander line UHF RFID reader antenna for near-field applications," *IEEE Transactions on Antennas and Propagation*, vol. 65, no. 1, pp. 82–91, 2017.

[3] R. Colella, L. Catarinucci, A. Michel, and P. Nepa, "Design of a 3D-printed circularly polarized antenna for portable UHF RFID readers," in *Proceedings of 2017 IEEE International Conference on RFID Technology & Application (RFID-TA)*, pp. 225–228, Warsaw, Poland, September 2017.

[4] S. Fu, C. Li, S. Fang, and Z. Wang, "Low-cost single-fed circularly polarized stacked patch antenna for UHF RFID reader applications," in *Proceedings of 2016 Progress in Electromagnetic Research Symposium (PIERS)*, pp. 2031–2034, Shanghai, China, August 2016.

[5] T. Tipsawate, C. Phongcharoenpanich, and S. Kosulvit, "A wideband bidirectional antenna using truncated circular sector fed by rectangular monopole," in *Proceedings of 6th International Conference on Electrical Engineering/Electronics, Computer, Telecommunications and Information Technology*, vol. 2, pp. 782–785, Pattaya, Chonburi, Thailand, January 2009.

[6] J. Y. Sze, C.-I. G. Hsu, Z. W. Chen, and C. C. Chang, "Broadband CPW-fed circularly polarized square slot antenna with lightening-shaped feedline and inverted-L grounded strips," *IEEE Transactions on Antennas and Propagation*, vol. 58, no. 3, pp. 973–977, 2010.

[7] J.-H. Lu and S.-F. Wang, "Planar broadband circularly polarized antenna with square slot for UHF RFID reader," *IEEE Transactions on Antennas and Propagation*, vol. 61, no. 1, pp. 45–53, 2013.

[8] R. Cao and S.-C. Yu, "Wideband compact CPW-fed circularly polarized antenna for universal UHF RFID reader," *IEEE Transactions on Antennas and Propagation*, vol. 63, no. 9, pp. 973–977, 2015.

[9] R. Xu, J.-Y. Li, and J. Liu, "Frequency-selective polarisation antenna based on simple rotational symmetric printed bow-tie dipole structure," *IET Microwaves, Antennas & Propagation*, vol. 12, no. 7, pp. 1107–1111, 2018.

[10] W.-H. Zhang, W.-J. Lu, and K.-W. Tam, "Circularly polarized complementary antenna with tilted beam based on orthogonal dipoles," *IEEE Antennas and Wireless Propagation Letters*, vol. 17, no. 8, pp. 1406–1410, 2018.

[11] W.-H. Zhang, W.-J. Lu, and K.-W. Tam, "Design of circularly polarized conical RFID reader antenna based on natural boundary conditions," *IEEE Journal of Radio Frequency Identification*, vol. 2, no. 2, pp. 104–110, 2018.

[12] U. Ullah and S. Koziel, "A geometrically simple compact wideband circularly polarized antenna," *IEEE Antennas and Wireless Propagation Letters*, vol. 18, no. 6, pp. 1179–1183, 2019.

[13] W. Abdelrahim and Q. Feng, "Compact broadband dual-band circularly polarised antenna for universal UHF RFID handheld reader and GPS applications," *IET Microwaves, Antennas & Propagation*, vol. 13, no. 10, pp. 1664–1670, 2019.

[14] Y. Pan and Y. Dong, "Low-profile low-cost ultra-wideband circularly polarized slot antennas," *IEEE Access*, vol. 7, no. 3, pp. 973–977, 2019.

[15] CST Microwave Studio Suite, *Computer Simulation Technology*, Dassault Systèmes Americas Corp., USA, 2019.